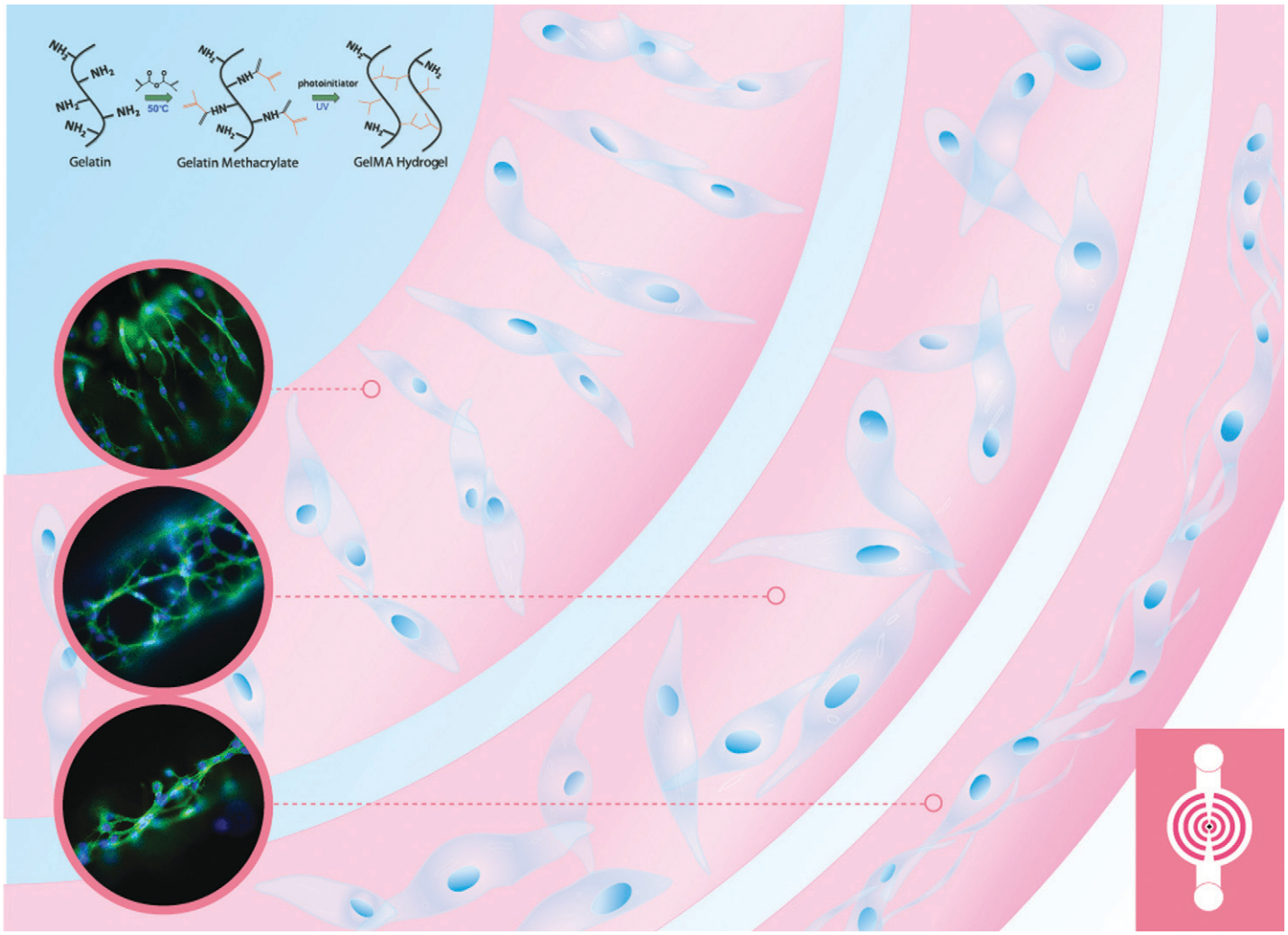


**Featuring work from the scientific collaboration between Prof. Ali Khademhosseini, in the Division of Biomedical Engineering, Brigham and Women's Hospital, USA and Prof. Fan-Gang Tseng, in the Department of Engineering and System Science, National Tsing Hua University, Taiwan**

Title: Gradient static-strain stimulation in a microfluidic chip for 3D cellular alignment

A simple and low-cost approach was developed using photopatternable concentric circular gelatin methacrylate (GelMA) hydrogel under the convex PDMS membrane in the microfluidic chip to simultaneously apply gradient static-strain on three-dimensional cell-laden hydrogels for the investigation of cellular behaviors.

## As featured in:


See Fan-Gang Tseng, Ali Khademhosseini *et al.*, *Lab Chip*, 2014, **14**, 482.

ROYAL SOCIETY OF CHEMISTRY

www.rsc.org/loc

Registered charity number: 207890

Lab on a Chip

PAPER

View Article Online
View Journal | View Issue

# Gradient static-strain stimulation in a microfluidic chip for 3D cellular alignment†

Cite this: *Lab Chip*, 2014, **14**, 482

Hsin-Yi Hsieh,‡[abc] Gulden Camci-Unal,§[bd] Tsu-Wei Huang,¶[e] Ronglih Liao,‖[f] Tsung-Ju Chen,**[a] Arghya Paul,††[bdg] Fan-Gang Tseng‡‡*[aeh] and Ali Khademhosseini§§*[bdg]



Received 27th July 2013,
Accepted 25th October 2013

DOI: 10.1039/c3lc50884f

www.rsc.org/loc

Cell alignment is a critical factor to govern cellular behavior and function for various tissue engineering applications ranging from cardiac to neural regeneration. In addition to physical geometry, strain is a crucial parameter to manipulate cellular alignment for functional tissue formation. In this paper, we introduce a simple approach to generate a range of gradient static strains without external mechanical control for the stimulation of cellular behavior within 3D biomimetic hydrogel microenvironments. A glass-supported microfluidic chip with a convex flexible polydimethylsiloxane (PDMS) membrane on the top was employed for loading the cells suspended in a prepolymer solution. Following UV crosslinking through a photomask with a concentric circular pattern, the cell-laden hydrogels were formed in a height gradient from the center (maximum) to the boundary (minimum). When the convex PDMS membrane retracted back to a flat surface, it applied compressive gradient forces on the cell-laden hydrogels. The concentric circular hydrogel patterns confined the direction of hydrogel elongation, and the compressive strain on the hydrogel therefore resulted in elongation stretch in the radial direction to guide cell alignment. NIH3T3 cells were cultured in the chip for 3 days with compressive strains that varied from ~65% (center) to ~15% (boundary) on hydrogels. We found that the hydrogel geometry dominated the cell alignment near the outside boundary, where cells aligned along the circular direction, and the compressive strain dominated the cell alignment near the center, where cells aligned radially. This study developed a new and simple approach to facilitate cellular alignment based on hydrogel geometry and strain stimulation for tissue engineering applications. This platform offers unique advantages and is significantly different from the existing approaches owing to the fact that gradient generation was accomplished in a miniature device without using an external mechanical source.

[a] *Institute of NanoEngineering and MicroSystems (NEMS), Department of Engineering and System Science, National Tsing Hua University, No. 101, Sec. 2, Kuang-Fu Rd., Hsinchu 30013, Taiwan R.O.C. E-mail: fangang@ess.nthu.edu.tw; Fax: +886-3-5720724; Tel: +886-3-5715131-34270*

[b] *Division of Biomedical Engineering, Department of Medicine, Brigham and Women's Hospital, Harvard Medical School, 65 Landsdowne Street, Cambridge, MA 02139, USA. E-mail: alik@rics.bwh.harvard.edu; Tel: +1-617-768-8395*

[c] *Department of Mechanical Engineering, National Taiwan University, No. 1, Sec. 4, Roosevelt Road, Taipei 10617, Taiwan, R.O.C.*

[d] *Harvard-MIT Division of Health Sciences and Technology, Massachusetts Institute of Technology, 77 Massachusetts Ave., Cambridge, MA 02139, USA*

[e] *Department of Engineering and System, National Tsing Hua University, No. 101, Sec. 2, Kuang-Fu Rd., Hsinchu 30013, Taiwan R.O.C.*

[f] *Cardiovascular Division, Department of Medicine, Brigham and Women's Hospital, Harvard Medical School, 77 Avenue Louis Pasteur, Boston, MA 02115, USA*

[g] *Wyss Institute for Biologically Inspired Engineering, Harvard University, 3 Blackfan Circle, Boston, MA 02115, USA*

[h] *Research Center for Applied Sciences, Academia Sinica, No. 128, Sec. 2, Academia Rd., Nankang, Taipei 11529, Taiwan R.O.C.*

† Electronic supplementary information (ESI) available: The dimensions of the PMMA mold and the molded PDMS membrane, pictures of the microfluidic chip with and without PDMS deformation, the calculation of the deformed PDMS curve, the approach for the cell alignment analysis, the comparison of the four circular hydrogel patterns (line-width/spacer of 50 μm/50 μm, 100 μm/100 μm, 200 μm/200 μm, and 300 μm/300 μm) for 3T3 cell encapsulation, and the comparison of the CSP and 3T3 cell behaviors under uniform strain stimulation. See DOI: 10.1039/c3lc50884f

‡ Authors' E-mail Addresses & Contributions: Hsin-Yi Hsieh (d9735803@oz.nthu.edu.tw): proposed the design of the gradient strain chip, performed and analyzed all the experiments, wrote the manuscript, and discussed the content with all other authors.

§ Gulden Camci-Unal (gcu@mit.edu): synthesized the GelMA, proposed the size effect for cell alignment, designed experiments, performed experiments, and revised and corrected the manuscript.

¶ Tsu-Wei Huang (d9511814@oz.nthu.edu.tw): designed the photomask and performed image analysis.

‖ Ronglih Liao (rliao@rics.bwh.harvard.edu): provided the CSPs and discussed the experimental results.

** Tsung-Ju Chen (peterchen810@gmail.com): provided the idea for the stretch stimulation of cells.

†† Arghya Paul (arghya.paul@gmail.com): performed the cell culturing.

‡‡ Fan-Gang Tseng (fangang@ess.nthu.edu.tw): designed the microfluidic chip and revised the manuscript.

§§ Ali Khademhosseini (alik@rics.bwh.harvard.edu): supervised the research, provided the hydrogel and revised the manuscript.

## Introduction

The ability to mimic the native microenvironments is crucial to introduce the formation of properly functioning tissue constructs.[1–6] Natural extracellular matrix (ECM) in the human body is a complex fibrous structure composed of various biomolecules, including bioactive binding proteins, biodegradable molecules, and signal-molecule binding sites to support cell growth and guide new tissue formation.[7–9] Natural hydrogels, such as hyaluronic acid (HA), chitosan, and alginate, usually require chemical modifications to include cell adhesive proteins for facilitating cell adhesion.[10–19] Alternatively, gelatin hydrogels with natural cell-binding motifs and matrix metalloproteinase-sensitive degradation sequences are promising materials for the reconstitution of biomimetic scaffolds in various tissue engineering applications.[20–25]

In combination with ECM hydrogels, biophysical stimulation has been suggested not only to regulate the various cellular functions related to stem cell differentiation and cell alignment[2,26,27] but also to improve cellular functions to mimic the biomechanical behaviors of natural tissues or organs, such as articular cartilage contraction, lung breathing, and heart beating.[28–30] One way to mimic the native tissue architecture is the ability to induce proper cellular alignment for propagation of small molecules and/or electrical signals in three-dimensional (3D) cell-laden hydrogels.[1–3,5,30–37]

Two most common approaches for cellular alignment are the regulation of the geometric topography[38,39] and the application of mechanical strain.[1,30,40,41] In biomimetic topography, cells align along the long-axis of a line pattern because of the confined free space in the direction of the short-axis.[38,39] For stimulation with compressive strain or elongation stretch, the mechanical constraint has been reported to align cells perpendicular to the direction of the compressive strain and parallel to the direction of the elongation stretch *in vitro*.[1,31,40] To facilitate tissue regeneration, it is essential to investigate cell alignment under possible force-loaded conditions similar to what happens in our bodies. Therefore, designing cell-laden hydrogels with different geometries is also a way of generating mechanical stimulation because biomechanical cues from external environments may have a more significant impact on the orientation of the cellular alignment than geometric guidance cues.[21,42]

Most of the previous studies have investigated cellular behavior by employing one strain condition at a time using complicated controlling systems, requiring mass sample preparation and complex experimental processes.[3,6,21,31,44] For example, Butcher *et al.* (2006) applied mechanical squeezing force on a chamber filled with liquid and cylindrical collagen disks to obtain a uniform compressive strain.[6] Gould *et al.* (2012) used elliptical compression springs to clamp anisotropic 3D collagen hydrogels in a biaxial strain bioreactor to control the ellipsoidal deformation ratio using step motors.[38] Such controlling equipment not only occupied a large volume in the incubator but also increased the risk of contamination.[6,43–46] Vader *et al.* (2009) and Marion *et al.* (2012) have dragged cell-laden collagen gels using pipette tips or elastic capillary rods to align collagen fibers for cellular alignment in standard cultural dishes. Although these methods are simple, it is challenging to precisely control the dragging force; thus, these approaches lack high reproducibility.[13,47] Given that cell-laden hydrogels are widely employed on the microscale for biomedical applications,[48–51] it is advantageous to combine micro-electro-mechanical systems (MEMS) approaches with a range of strain/stretch stimuli to simultaneously investigate cell behaviors in 3D biomimetic constructs *in vitro*.[2,4,33] For instance, Moraes *et al.* (2011) and Park *et al.* (2012) have varied the gas pressure on the PDMS membrane in microfluidic chips to obtain various strains to study cellular deformation or drive differentiation of cells into different lineages.[44,51] However, these approaches presented technical challenges with chip fabrication, software control of motors, pumps, and valves, and compressed gases.

Thus, in this work, we developed a simple approach to create a self-sustaining gradient-static-strain microfluidic chip (GSS-microChip) by employing a concentric circular hydrogel pattern and a flexible PDMS membrane. Unlike most of the existing platforms, our GSS-microChip is a portable and disposable miniature device that can self-generate gradient forces on concentric cell-laden hydrogels without the need for external mechanical equipment. In this paper, we present the basic operating principles of this GSS-microChip, including the calculation of the strain gradient with or without cell encapsulation. We also present the results of our experiments using 3T3 fibroblast cells that were aligned by the hydrogel geometry and/or hydrogel elongation under a variety of static strain conditions within 3D ECM-mimetic environments. This platform offers unique advantages compared to current tissue engineering approaches due to the simple fabrication and operation processes to self-generate gradient strains in a disposable and miniature microfluidic device.

## Experimental

### 1. Materials

The chemicals for the synthesis of the methacrylated gelatin (GelMA) (gelatin (gel strength 300, type A, from porcine skin) and methacrylic anhydride) and the surface modification of the glass slides ((3-trimethoxysilyl)propyl methacrylate (TMSPMA)) for hydrogel immobilization were all purchased from Sigma-Aldrich, USA. The glass slides were purchased from Fisher Scientific, USA. The 400 nm Fluoro-Max™ fluorescent polystyrene beads (G400) were obtained from Thermo Fisher Scientific, Inc., USA. The photomasks were supplied by Taiwan Kong King, Taiwan, and the UV light source (Omnicure S2000) was obtained from EXFO Photonic Solutions Inc., Canada. Various thicknesses of PMMA, including 700 μm, 1 mm, 1.5 mm, and 2 mm, were purchased from Taiwan for the fabrication of PMMA molds.

### 2. Cell culture

All cells were cultured in a standard cell culture incubator (Forma Scientific) in a 5% $CO_2$ atmosphere at 37 °C. The culture medium used for NIH 3T3 fibroblast was Dulbecco's modified Eagle medium (DMEM; Gibco) supplemented with 10% fetal bovine serum (FBS; Hyclone) and 1% penicillin–streptomycin (Pen–Strep; Gibco). The cells were passaged twice per week. Cardiac side population cells (CSPs) were received as described previously[52] and cultured in minimum essential medium alpha (MEM α; Gibco) supplemented with 20% FBS, 1% Pen–Strep. The CSPs were passaged when they reached 60–70% confluence and were used at passage 6 or 7 for cell encapsulation studies.

### 3. GelMA synthesis

The GelMA was synthesized as previously described.[2,14] Briefly, 10 g of gelatin powder was dissolved in 100 mL of DPBS and mixed with a magnetic rotator on a hot plate at 50 °C until the gelatin powder was completely dissolved. After the gelatin had dissolved, 8 mL of methacrylic anhydride was added dropwise and reacted at 50 °C for 3 h. Next, 400 mL of DPBS was added into the flask to dilute the GelMA solution. The final solution was then dialyzed within 12–14 kDa cutoff dialysis tubing (Spectra/Por molecular porous membrane tubing, MWCO 12–14 kDa, Fisher Scientific) in distilled water for 1 week at 40 °C and subsequently lyophilized for 1 week.

### 4. Chip fabrication

The GSS-microChips were fabricated by binding a TMSPMA-coated slide with a PDMS sheet that had been demolded from a PMMA mold, as shown in Fig. S-1.† The PMMA master mold (Fig. S-1†) for the PDMS molding was assembled from several pieces of PMMA that had been cut using a $CO_2$ laser. The final dimensions of the circular PDMS membrane were 12 mm in diameter and 1.5–2.0 mm thick with a 300 μm-deep trench. After bonding, the GSS-microChip had the following dimensions: 25 mm ($W$) × 37.5 mm ($L$) × 3 mm ($H$).

### 5. Cell encapsulation and micropatterning

Cell-laden GelMA hydrogels were photopatterned onto TMSPMA-coated glass slides. Briefly, as shown in Fig. 1(a)–(b), 100 μL of prepolymer cell suspension (5% GelMA (w/v) prepolymer, 0.1% photoinitiator, and 3 × $10^6$ cells per mL) was pipetted into the inlet of the microfluidic chip (Fig. 1(a)). When the flow channel and the center chamber were fully filled with cell-loaded prepolymer, a micropipet containing 50 μL of cell-laden prepolymer cell suspension was placed into the inlet through an L-shaped tube with a valve. Then, a PDMS plug was used to block the outlet of the flow channel. The liquid pressure applied on the PDMS membrane was released prior to injecting the 10–50 μL injection volume ($V$) from the micropipet to induce PDMS deformation. Next, the chip was flipped, and the photomask with a concentric circular pattern was placed on top of the glass slide. The region of

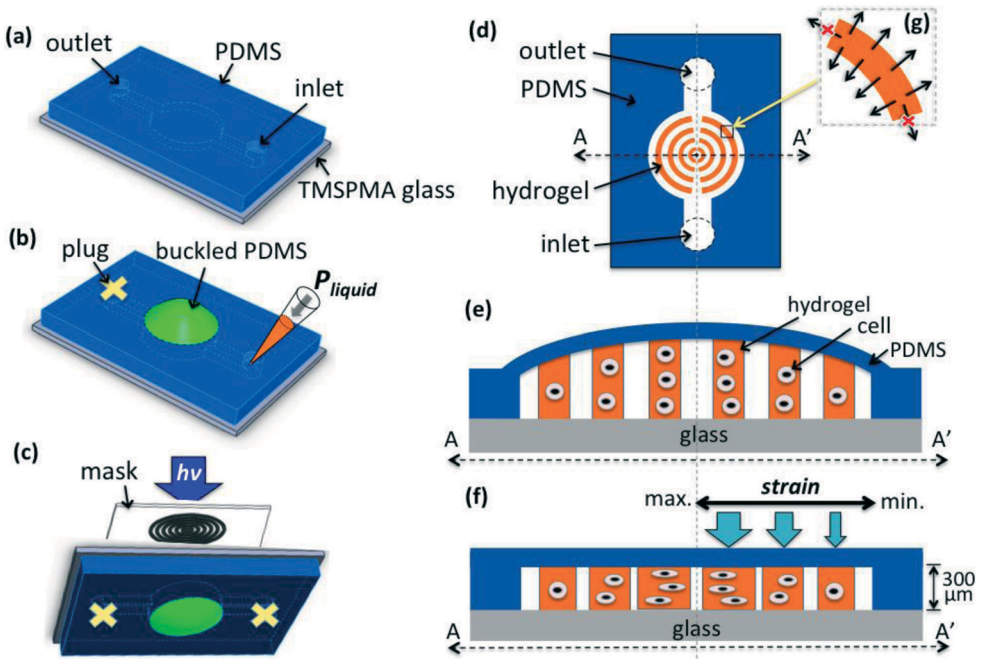


Fig. 1 Schematic of the fabrication processes for gradient strain hydrogels in a microfluidic chip. (a) PDMS was bonded to the TMSPMA-coated glass. (b) A PDMS plug was used to block the outlet and application of liquid pressure to obtain convex PDMS deformation. (c) After UV patterning through the glass bottom, the uncrosslinked hydrogel with cells was washed out, and (d) concentric circles were formed in the chip with (e) a height gradient along the radius. (f) The inlet and outlet were unplugged, and the PDMS membrane became flat and applied gradient force on the cell-encapsulated hydrogels. (g) The stretch direction of the circular hydrogel under strain or stress due to the PDMS membrane after releasing the liquid pressure.

 

the circular pattern was then exposed to 6.9 mW $cm^{-2}$ UV light (320–500 nm) for 50 s (Fig. 1(c)). Following polymerization, the PDMS plug and the micropipet were removed. Subsequently, the remaining unpolymerized prepolymer was gently washed away with 3 mL of pre-warmed DPBS solution. Micropatterned, cell-laden hydrogels were cultured in the specified media for up to 5 days at 37 °C with 5% $CO_2$ in air atmosphere, and the media were replenished every day. To visualize the micropatterns, 400 nm fluorescent polystyrene beads were mixed with GelMA prepolymer without cells at a concentration of 0.01% (w/v) prior to UV exposure to produce fluorescent hydrogels.

### 6. Cell viability assay

The cellular viability of the specimens was assessed by incubating them in a solution of 2 μg $mL^{-1}$ calcein AM (Molecular Probes, USA) and 5 μg $mL^{-1}$ propidium iodide (P4170, Sigma-Aldrich) for 15 min. Green fluorescence from live cells was due to the activation of calcein AM by intracellular esterase activity, and red fluorescence stained dead cells, due to the permeation and binding of propidium iodide to the nucleic acids of membrane-compromised cells.

To stain the cell nuclei and actin filaments, the cells were fixed with 4% paraformaldehyde in Dulbecco's phosphate buffered saline (DPBS) for 15 min, followed by permeabilization with 0.5% Triton X-100 in PBS for 10 min. Then, the samples were blocked in 1% BSA solution for 45 min at room temperature[53,54] and exposed to Alexa Fluor 488 phalloidin (A12379, Invitrogen) for 1 h at 37 °C, and 1 μg $mL^{-1}$ 4′,6-diamidino-2-phenylindole dihydrochloride (DAPI; Sigma) for 5 min. Fluorescent images for each sample were captured using an inverted fluorescence microscope (Olympus IX70) with ex/em at 490/515 nm, 535/617 nm, 488/520 nm, and 358/461 nm for calcein AM, propidium iodide, Alexa Fluor 488 phalloidin, and DAPI, respectively.

### 7. Quantification of cell alignment

At various times up to 5 days in culture, the cell-laden hydrogels in the fluidic chip were stained to assess cellular viability using calcein AM/propidium iodide and to visualize the cytoskeleton and nuclei using phalloidin (Alexa-Fluor 488) and DAPI according to the manufacturer's instructions. The cell viability, cell shape factor, and alignment of the nuclei were measured using the ImageJ software to quantitatively assess the numbers of live and dead cells and evaluate overall cell elongation and alignment.

The cell viability was calculated as viability = (number of green cells/total number of green and red cells) × 100%. The shape factor was calculated as roundness = 4 × π × area/perimeter$^2$.[2,55] The value of the shape factor varied between 1 (circular shape) and 0 (elongated, linear morphology). The relative orientation of cell nuclei in the DAPI staining images was used to measure the cell alignment angle. The nuclear angle was defined as the orientation of the major elliptical axis of each nucleus with respect to the horizontal axis.

All nuclear angles were then converted into the new coordinate system; the angle along the radial direction was 90°, and the angle along the circular periphery was 0° or 180°. For alignment analysis, the nuclear angles were grouped in 10° increments, and the cells with preferred nuclear angles within less than 20° were considered to be aligned.[39–41] Thus, the cells with angles in the range of 70° to 110° were considered aligned along the radial direction, and the cells with angles in the range of 0° to 20° and 160° to 180° were considered aligned along the arc direction of the circle (circular alignment). We defined the radial-to-circular alignment ratio ($RCA_{ratio}$) as the number of cells aligned radially divided by number of cells aligned along the circular direction. The $RCA_{ratio}$ value is ~1 when the average alignment is random. If the value is much larger (or smaller) than 1, then there is more radial (or circular) alignment than circular (or radial) alignment.

All quantified values including cell viability, circularity, viable cells per millimeter, and the radial-to-circular alignment ratio, of each sample were obtained from 4 replicates.

## Results and discussion

### 1. Principles of the GSS-microChip

The distinguishing feature of our GSS-microChip is the application of a gradient force to the cell-encapsulated hydrogel without the need for an external device. Therefore, after UV crosslinking, the chip can be placed directly in a Petri dish and cultured in an incubator to study cellular behavior as a function of time.

The principle of the gradient chip is shown in Fig. 1. The GSS-microChip was fabricated by binding a molded PDMS membrane to TMSPMA-coated glass (Fig. 1(a)). To exert gradient strain on the hydrogel, the flow channel of the chip was first filled with the prepolymer–cell suspension (Fig. S-1(a)†), and then a PDMS plug was used to close the outlet of the flow channel. A micropipet containing 50 μL of prepolymer cell suspension was connected to the inlet of the chip with an L-shape tube. The prepolymer cell suspension was gently injected into the chip. Due to the elastic nature of the PDMS membrane, the injected volume ($V$) from the micropipet exerts liquid pressure, applying force to the PDMS membrane and causing deformation (Fig. S-2(b)†). Increasing the liquid volume ($V$) results in an increase in the extent of PDMS deformation, and a decrease in the radius of curvature ($r$) of the convex PDMS membrane. The chip described above, with one end with a PDMS plug and the other end attached to a micropipet, was placed upside down for hydrogel crosslinking by UV exposure through a photomask with a concentric circular pattern (Fig. S-3(a)†). After opening both ends of the flow channel and washing away the uncrosslinked prepolymer cell suspension, cell-encapsulated circular hydrogels were formed, as shown in Fig. 1(d) and S-2(c).†

Cross-sectional views of the A–A′ before and after opening the inlet or outlet are shown in Fig. 1(e) and (f), respectively (the uncrosslinked residue was omitted). After UV exposure and before opening the inlet or the outlet, the concentric

circular hydrogels had different heights because of the convex PDMS membrane (Fig. 1(e)). The circular hydrogels in the GSS-microChip have a height gradient that decreases from the center to the outer boundary. After the inlet or outlet was opened, the liquid pressure applied to the PDMS membrane was released. Thus, the buckled PDMS membrane returned to a (nearly) flat state, and it applied a compressive strain gradient to the circular concentric hydrogels (Fig. 1(f)). The continuous hydrogel is confined in the circular direction; therefore, it can only elongate along the radial direction when experiencing force from the PDMS membrane (Fig. 1(g)).

### 2. Calculation of the gradient strain

The principle of gradient strain hydrogels is based on the convex curve of the PDMS membrane generated by the over-injection of uncrosslinked prepolymer cell suspension. Poisson's ratio —the ratio of the contraction (or extension) in the direction perpendicular to the applied load to the stretched (or compressed) deformation in the direction of the applied load—of the cell-laden prepolymer suspension was assumed to be 0.5,[15,56] which fixes the total volume of the prepolymer solution. Therefore, the injected volume ($V$) from the micropipet will deliver liquid pressure to the wall of the flow channel between the PDMS membrane and the glass. The 12 mm flexible PDMS membrane in the chip is the easiest region to be deformed to reduce the liquid pressure from the injected volume ($V$), and we assumed that there was no deformation other than that of the 12 mm PDMS circle. Thus, the injected volume ($V$) equals the volume of over-injection in the region shown in pink (Fig. 2(a)).

By calculating the relationship between the PDMS deformation curve and the injected volume ($V$) (details in the ESI, Fig. S-4†), the value of the curvature and the maximum height ($H_0$) of the deformed PDMS membrane were determined and are shown as the black line in Fig. 2(b). The experimental results for the maximum height of the deformed PDMS membrane, shown in Fig. 2(b), were obtained by measuring the position of the membrane before and after the injection volumes of DI water. The experimental data matched the calculation curve consistently, verifying that our calculation model for the PDMS deformation curve is suitable for an incompressible solution, such as water (most hydrogels have the same Poisson's ratio such as water).

In our concentric circular hydrogel pattern, the compressive strain and elongation originated from the squeezing force exerted by the retracted convex PDMS membrane. When the PDMS membrane compresses the hydrogel (Fig. 2(c), in white) along the $H$-axis, the circular hydrogel elongates (Fig. 2(c), in blue) along the radial-axis. Before the GSS-microChip experiments were performed, four photomask sizes (the width/spacer dimensions of 50 μm/50 μm, 100 μm/100 μm, 200 μm/200 μm, and 300 μm/300 μm) were compared as described in the ESI,† section D to G, with uniform compressive strain.

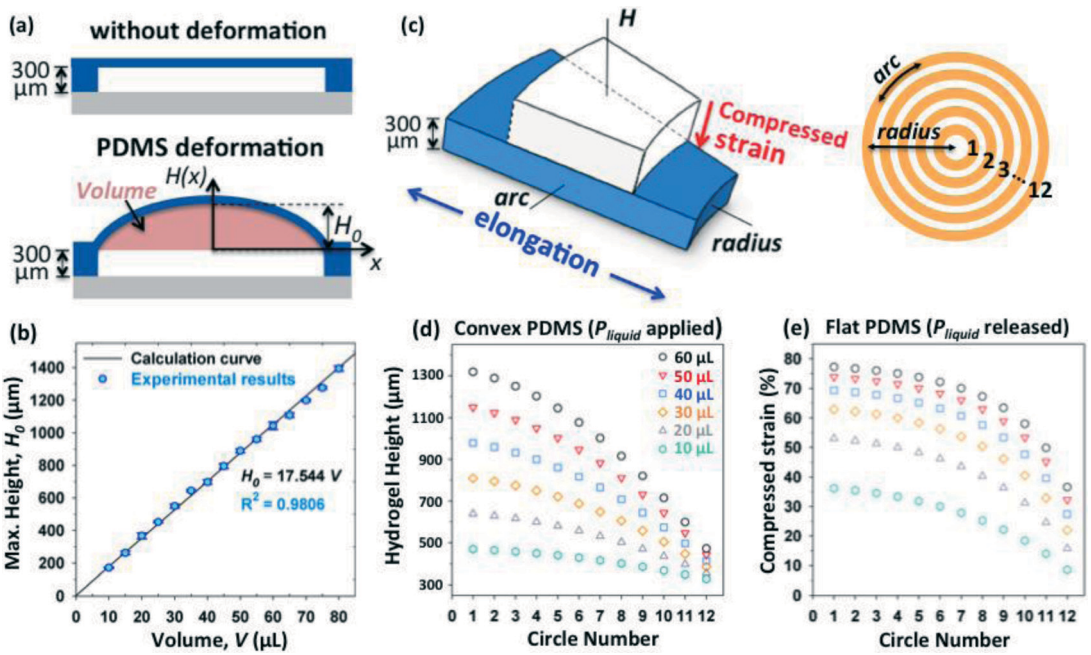


**Fig. 2** Calculated and/or experimental data for the correlations among the injection volume ($V$), the maximum height of the deformed PDMS membrane ($H_0$), the height of the concentric hydrogel circles ($H(x)$ + 300 μm) before releasing liquid pressure, and the compressive strain and tensile stretch percentages after releasing liquid pressure ($P_{liquid}$). (a) Schematic illustration of the PDMS deformation and the definition of the coordinates by the volume of hydrogel injection. (b) Calculated and experimental data for the correlation between the injected volume, $V$, and the maximum height of the PDMS deformation, $H_0$. (c) The definition of compressive strain and the stretch of the concentric circular hydrogels under the stress exerted by the PDMS membrane. The circle number represents the number of concentric hydrogel circles from the center to the outer boundary. (d) Calculated results for the height of the concentric hydrogel circles under the convex PDMS membrane, and (e) the compressive strain percentages of the concentric hydrogel circles after releasing the liquid pressure.

 

Two cell types, 3T3 cells and cardiac side population (CSP) cells, were also analyzed for their cell viability, cell alignment ratio ($RCA_{ratio}$), viability, and cell circularity. After the cellular behavior was compared under conditions of uniform compressive strain, the photomask size of 200 μm (referring to Fig. S-3†) was selected for the GSS-microChip. The photomask size of 200 μm with two fan-shape openings (Fig. S-3(a)†) was only used for GSS-microChip, and the full concentric circular patterns with 50, 100, 200, and 300 μm pattern sizes (Fig. S-3(b)†) were only used for the experiments with uniform compressive strain in the supporting data.

There were 12 hydrogel circles under the PDMS membrane in the gradient chip, and the numbers from the center to the boundary are referred to as numbers 1 through 12 (Fig. 2(c)). Thus, the hydrogel height could be evaluated as shown in Fig. 2(d) and section C of Fig. S-4.† To obtain the compressive strain percentage in Fig. 2(e), the percentage of $(H(x) - 300)/H(x)$ was calculated for hydrogels 1 to number 12 by employing different injection volumes. Here, we assumed the PDMS would return to a flat state; therefore, the final height of the compressed hydrogels was 300 μm.

### 3. Gradient elongation without cell encapsulation

For incompressible materials (with Poisson's ratio of 0.5), the compressive strain of the material in one axis will be converted to elongation in the other two axes with half of the compressive strain value. However, the design of the circular hydrogel confines the extension of the hydrogel upon exposure to compressive forces. The concentric hydrogels are able to elongate along the radial direction (Fig. 1(g) and 2(c)). As a result, the maximum elongation of the hydrogel along the radial axis is the same as the compressive strain of the incompressible material.

In this section, the elongation gradient was studied using 5% GelMA, 0.1% photoinitiator, and 0.01% G400 PSBs. The images in Fig. 3(a), (b), and (c) show the patterned circular hydrogels at day 0 in the GSS-microChip with 0, 20 and 40 μL

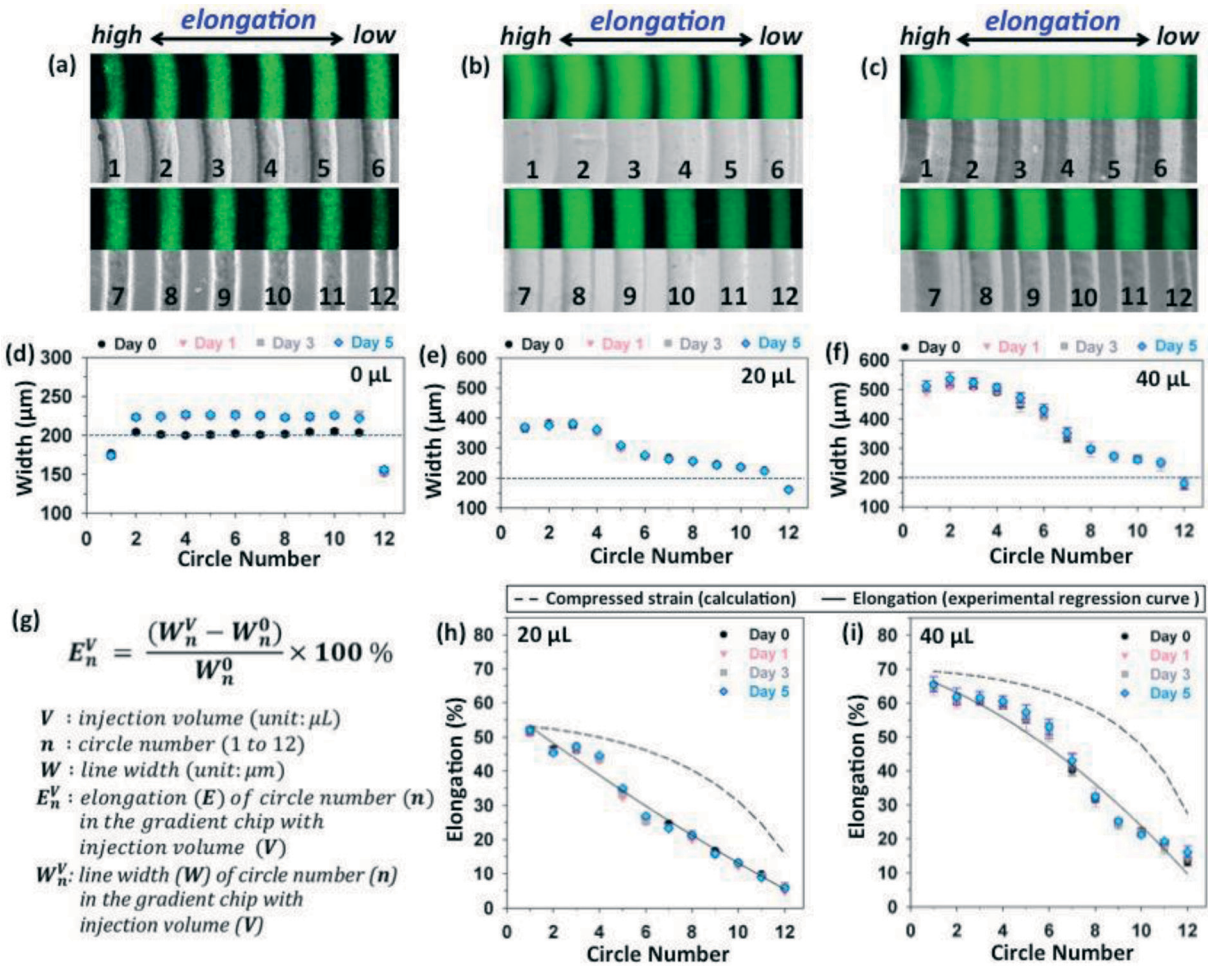


Fig. 3 Hydrogel elongation in the GSS-microChip by the 0 μL (control group), 20 μL, and 40 μL injection volumes (without cell encapsulation). Fluorescence and phase contrast images of circular hydrogels in the chips with (a) 0 μL, (b) 20 μL, and (c) 40 μL injection volumes. The hydrogel was a mixture of 5% GelMA, 0.1% photoinitiator, and 0.01% 400 nm fluorescence beads. The line widths (*W*) of the circular hydrogels at different days in the chips with (d) 0 μL, (e) 20 μL, and (f) 40 μL injection volumes. (g) The formula for the calculation of the elongation percentage. The elongation percentage of the hydrogels in the chips with (h) 20 μL and (i) 40 μL injection volumes.

injection volumes, respectively. The line widths of the circular hydrogels from day 0 to day 5 in the chips with 0, 20, and 40 μL injection volumes are shown in Fig. 3(d), (e), and (f), respectively. The results indicate that different injection volumes caused different elongation gradient curves.

For the hydrogels with the 0 μL injection volume (control group), the line widths of hydrogels 2–11 were the same as the photomask size, 200 μm, at day 0. Starting from day 1, the line width expanded approximately 10%, resulting from the swelling of the hydrogel in the DPBS solution. Hydrogels 1 and 12 were smaller than the others. One possible reason is that the UV light passing through the photomask experienced interference and diffraction effects.[57,58] Therefore, the UV intensity for each hydrogel circle was determined by integrating the UV energy from the corresponding pattern number of the photomask and the neighboring circular patterns (Fig S-13†). Hydrogels 1 and 12 were at the boundaries, so the integrated UV intensities for hydrogels 1 and 12 were smaller than those for hydrogels between 2 and 11 (Fig. S-13†).

For the hydrogels in the GSS-microChips with 20 and 40 μL injection volumes (Fig. 3(e) and (f)), the results verified that the principle of the GSS-microChip successfully generated gradient elongation in the concentric circular hydrogels with a gradually decreased line width from number 1 to number 12. The concentric hydrogels did not significantly swell in the chips with the 20 μL and 40 μL injection volumes. To calculate the elongation percentage, we developed the formula given in eqn (1) and Fig. 3(g) based on the control group of hydrogels without compressive stress stimulation (0 μL injection volume in GSS-microChip).

$$E_n^V = \frac{\left(W_n^V - W_n^0\right)}{W_n^0} \times 100\% \quad (1)$$

In brief, the elongation ($E_n^V$) is the difference between the line width of hydrogel number $n$ in the chip with a $V$ μL injection volume and the line width of the number $n$ hydrogel in the chip with the 0 μL injection volume ($W_n^V - W_n^0$) divided by the line width of the number $n$ hydrogel in the chip with the 0 μL injection volume ($W_n^0$).

The elongations of the hydrogels in the chips with 20 μL and 40 μL injection volumes are shown in Fig. 3(h) and (i), respectively. The black line is the regression line for the elongation curve, and the dashed line is the calculated compressive strain from Fig. 2(e), which also represents the ideal elongation curve for incompressible materials. The experimental elongation values were smaller than the calculated values from the curve, and the first several hydrogels had experimental elongation values closer to the calculated results. The mismatch between the calculated and experimental results is potentially due to the partial extension of the hydrogel circle along the circular direction (please see the ripple, which represents the increased length of the hydrogel circle in Fig. S-5†) and the slightly raised PDMS membrane. The PDMS membrane was assumed to return back to the flat state when calculating the compressive strain, but the PDMS membrane did not completely retract back to the flat state. The hydrogels in the center area resisted to the force from the PDMS membrane, and therefore, the PDMS membrane was slightly lifted in the center after releasing the liquid pressure from the inlet and outlet.

## 4. Gradient elongation with cell encapsulation

When producing gradient hydrogels in the chip, we also compared several injection volumes of hydrogels for 3D cell encapsulation and monitored the changes in the hydrogels from day 0 to day 5. For the gradient hydrogels without cells (Fig. 3), the widths of concentric hydrogels in the chips with the 20 μL or 40 μL injection volume from the center to the boundary were consistent from day 0 to day 5. However, the hydrogel underwent a shrinkage process over time when the hydrogels were encapsulated with 3T3 cells, as shown in Fig. 4(a).

In step one at day 0 (Fig. 4(a)), the cell-loaded hydrogel was crosslinked, and the black line represents the boundary of the originally crosslinked hydrogel. When the PDMS membrane applied force to the hydrogel, the hydrogel extended in the radial direction and became elongated in the blue area (Fig. 4(a)). The elongation of hydrogel guided cells to align along the radial direction. Therefore, in step two, cells were gradually spreading in a radial direction. However, the spreading cells were also pulling on the hydrogels. As a result, in step 3, the cell contraction reduced the degree of hydrogel elongation in the radial direction. The shrinkage process basically repeated the cell spreading and pulling on hydrogel in radial direction (step 2) and the reduction of hydrogel elongation (step 3) over time.

Although 20 μL injection volume had an obvious gradient elongation curve (Fig. 3(h), without cell encapsulation), the shrinkage of hydrogel elongation due to cell spreading resulted in the disappearance of the gradient elongation curve at day 3 or day 5. As shown in Fig. 4(b) and (c), the 20 μL injection volume at day 0 resulted in a complete elongation gradient, but the shrinkage phenomenon significantly reduced the hydrogel elongation gradient at day 3. As shown in sections E, F, and G, in the ESI (Fig. S-10(b), S-11(b), and S-12†), it took 3 days to achieve cell spreading and alignment.[19,50] Therefore, we injected a larger volume, 40 μL, to compensate for the shrinkage originating from cell spreading because the slightly raised PDMS membrane in the GSS-microChip with a 40 μL injection volume can maintain sufficient force on the hydrogel circles to promote cellular alignment.

As shown in Fig. 4(d) and (e), the hydrogel elongation gradient appeared at day 0 and remained at day 3 after gel shrinkage. The line widths of the hydrogel circles from day 0 to day 5 were also calculated for the chips with 20 μL and 40 μL injection volumes and are shown in Fig. 4(f) and (g), respectively. As shown in Fig. 4(g), line widths of hydrogels 2–5 were greater than 400 μm. Because it is difficult to obtain clear boundaries for the hydrogels encapsulated with cells, the line width of any hydrogel that came in contact with the neighboring hydrogels was considered to be 400 μm.

 

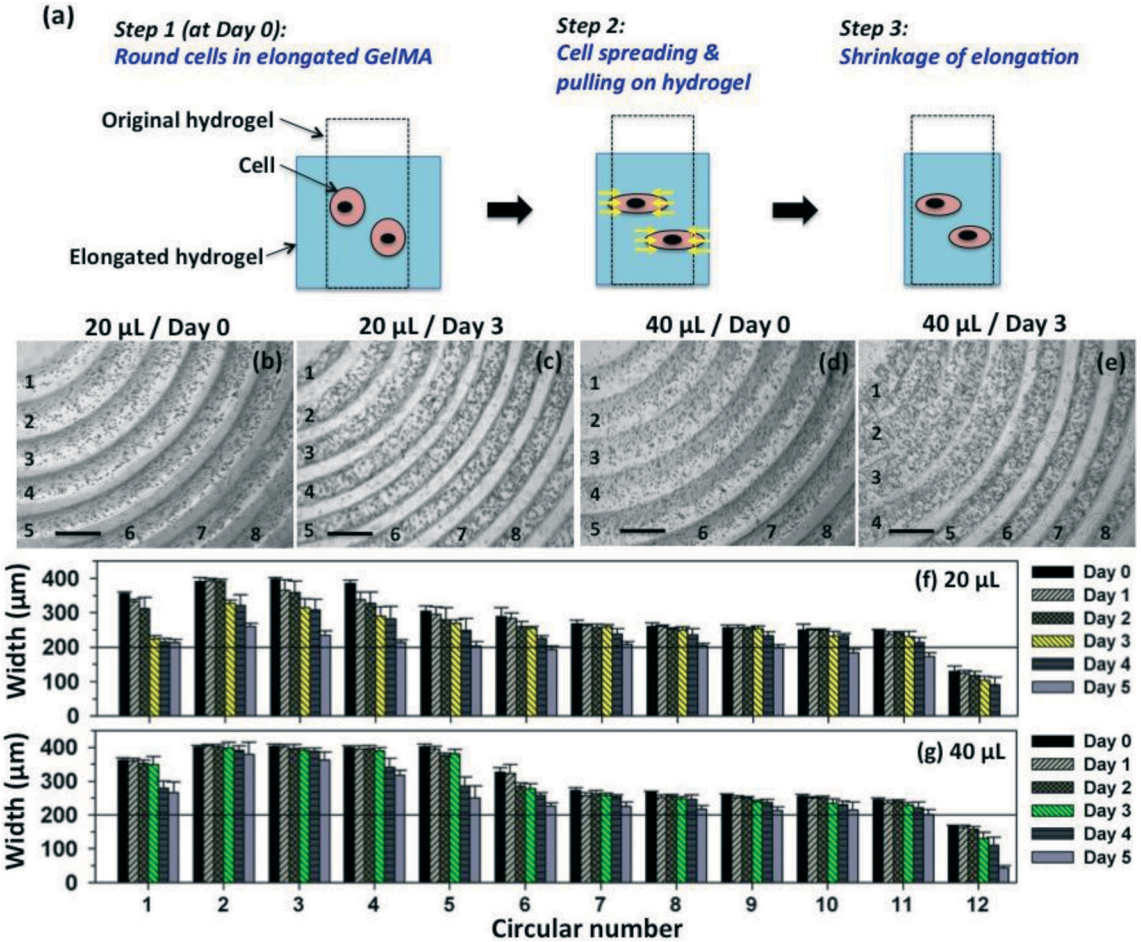


**Fig. 4** The shrinkage of hydrogel elongation with encapsulated 3T3 cells. (a) Schematic illustration of the shrinkage process over time. Phase contrast images for (b) the 20 μL injection volume at day 0, (c) the 20 μL injection volume at day 3, (d) the 40 μL injection volume at day 0, and (e) the 40 μL injection volume at day 3. The line widths of the concentric hydrogels with 3D cell encapsulation in the chips with (f) 20 μL and (g) 40 μL injection volumes. Scale: 100 μm.

The change in the line widths of the hydrogels was also in agreement with the gel shrinkage phenomenon because the line width gradually decreased for each hydrogel. Because the cell density decreased from hydrogel 1 to hydrogel 12, the shrinkage phenomenon (or the decreasing slope of the hydrogel width) is more obvious in the hydrogels near the center, especially numbers 1–4. The current design of GSS-microChip inevitably results in non-uniform cell density distribution across the concentric rings. Therefore, the cell density factor cannot be separated from the shrinkage phenomenon. For the 50 μL injection volume, the hydrogel elongation gradient could be still maintained from day 0 to day 5, but there were problems with diffusion in the fluorescent staining (data not shown). The calcein AM solution could not diffuse through the hydrogels in the center-most six circles in the chip with the 50 μL injected volume. Therefore, the 40 μL injection volume was selected for the GSS-microChip.

## 5. Cell alignment trend

The cell alignment was analyzed by staining the cell nuclei and F-actin with DAPI and phalloidin, respectively. The DAPI staining provided the information on each cell's nuclear angle, and the phalloidin staining was used to assess cell spreading and orientation. For the cell alignment analysis, we employed circular 3T3-laden hydrogels exposed to uniform strain to build up the analysis approach (see section E, Fig. S-9 and eqn (S-1), ESI†). For cell alignment in the GSS-microChip, as shown in Fig. 5(a), (b), and (c), the 3T3 cells aligned along the radial direction in hydrogel 1, the cells aligned randomly in hydrogel 7, and the cells aligned along the circular direction in hydrogel 12. Based on the DAPI/phalloidin staining images, it is obvious that the cell alignment angle of the 3T3 cells in hydrogel 1 (maximum hydrogel elongation in the radial direction) was a 90° shift from the alignment angle of the cells with long-axis alignment in hydrogel 12 (lowest hydrogel elongation in the radial direction).

The frequencies of the 3T3 cell nuclear angles in hydrogels 1, 7, and 12 were also analyzed, and the results are shown in Fig. 5(d), (e), and (f), respectively. The nuclear angles were converted into the new coordinate system; that is, 0 or 180° indicates that the long axis of the cell nucleus is parallel to the hydrogel circle (circular alignment), and 90° indicates that

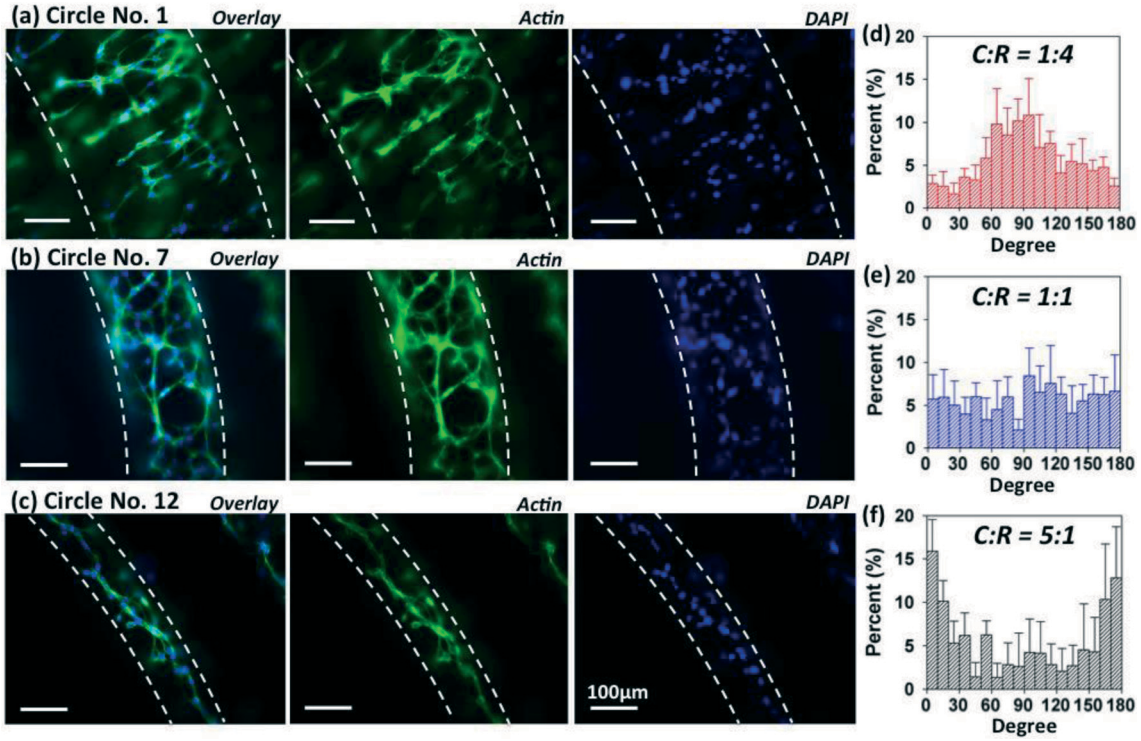


**Fig. 5** Actin–DAPI staining images and the alignment frequency of the 3T3 cells in the gradient chips at day 3. The analysis of the compressive strain and/or elongation of 5% GelMA with encapsulated cells for (a) circle 1, (b) circle 7, and (c) circle 12 revealed that the circle-to-radius ratios for these circles were (d) 4, (e) 1, and (f) 1/5, respectively. Scale: 100 μm.

the long axis of cell nucleus is perpendicular to the hydrogel circle (radial alignment). The $RCA_{ratio}$ was 4, 1, and 1/5 for the 3T3 cells in hydrogels 1, 7, and 12, respectively, in the GSS-microChip with the 40 μL injection volume. The approach for calculating $RCA_{ratio}$ is presented in eqn (S-1) in the ESI.†

In previous studies,[2,59,60] cell-encapsulated 200 μm line-patterned hydrogels were aligned along the long-axis direction of the hydrogel. When we applied an elongated stretch on the 200 μm hydrogels in the short-axis direction, the cell alignment angle was affected. In the GSS-microChip, the long-axis effect of geometric guidance (cell spreading along the long axis of the hydrogel line pattern) and the elongation stretch (cell spreading along the elongated direction of the hydrogel) compete to guide the overall cell alignment angle. For hydrogel 1, the elongation stretch of the hydrogel dominates the cell alignment. For number 12 hydrogel, the long-axis effect of hydrogel dominated the cell alignment. For hydrogel 7, the elongation stretch of the hydrogel neutralized the long-axis effect of geometric guidance, and the 3T3 cells randomly aligned and spread in the hydrogel. The long-axis effect for cell alignment is related to the cell size in the same width of line-patterned hydrogel. In section G and Fig. S-12 in the ESI,† CSPs and 3T3 cells were compared based on their cell size and alignment. In brief, CSPs, which were 124 μm in length and had an $RCA_{ratio}$ of ~0.2 at day 5 (strain-free in Fig. S-12(d)†), aligned much more along the long-axis of the hydrogel circle than the 3T3 cells, which were 52 μm in length and had an $RCA_{ratio}$ of ~1 at day 5 (strain-free in Fig. S-10(b),† 200 μm/200 μm). Therefore, the ratio of the cell size to the hydrogel width seems to be an important factor that affects the long-axis alignment in 3D hydrogels.

To demonstrate the continuous gradient strain/elongation in the chip, the $RCA_{ratio}$ of each circular hydrogel in the chips with 0 μL and 40 μL injection volumes at day 0 and day 3 are shown in Fig. 6. In this figure, the $RCA_{ratio}$ values of the cells in hydrogels 1 to 12 in the chip with the 40 μL injection volume at day 0 were not significantly different. It takes approximately three days for the cells to re-arrange their angles, and the $RCA_{ratio}$ values of the cells in the chip with the 40 μL injection volume at day 3 continuously decreased from hydrogel 1 to hydrogel 12 (Fig. 6(c)). For the 40 μL injection volume, only hydrogels 1, 4, 7, 10, and 12 were analyzed to identify significant differences. Almost all the $RCA_{ratio}$ values of the cells in hydrogels 1, 4, 7, 10, and 12 were significantly different, and the $RCA_{ratio}$ values of the cells gradually decreased from hydrogels 1 to 12. Compared with the $RCA_{ratio}$ values of the control group, that is, the cells in the chip with the 0 μL injection volume at day 0 (Fig. 6(b)), the $RCA_{ratio}$ values of the cells in the 40 μL/day 0 condition were not significantly different. However, the values for hydrogels 1 to 7 were significantly different between the 40 μL/day 3 (Fig. 6(c)) and 0 μL/day 3 (Fig. 6(d)) conditions. For the 0 μL injection volume, all hydrogels are analyzed to identify statistically significant differences. (The symbol of "#" was used to denote a significant

 

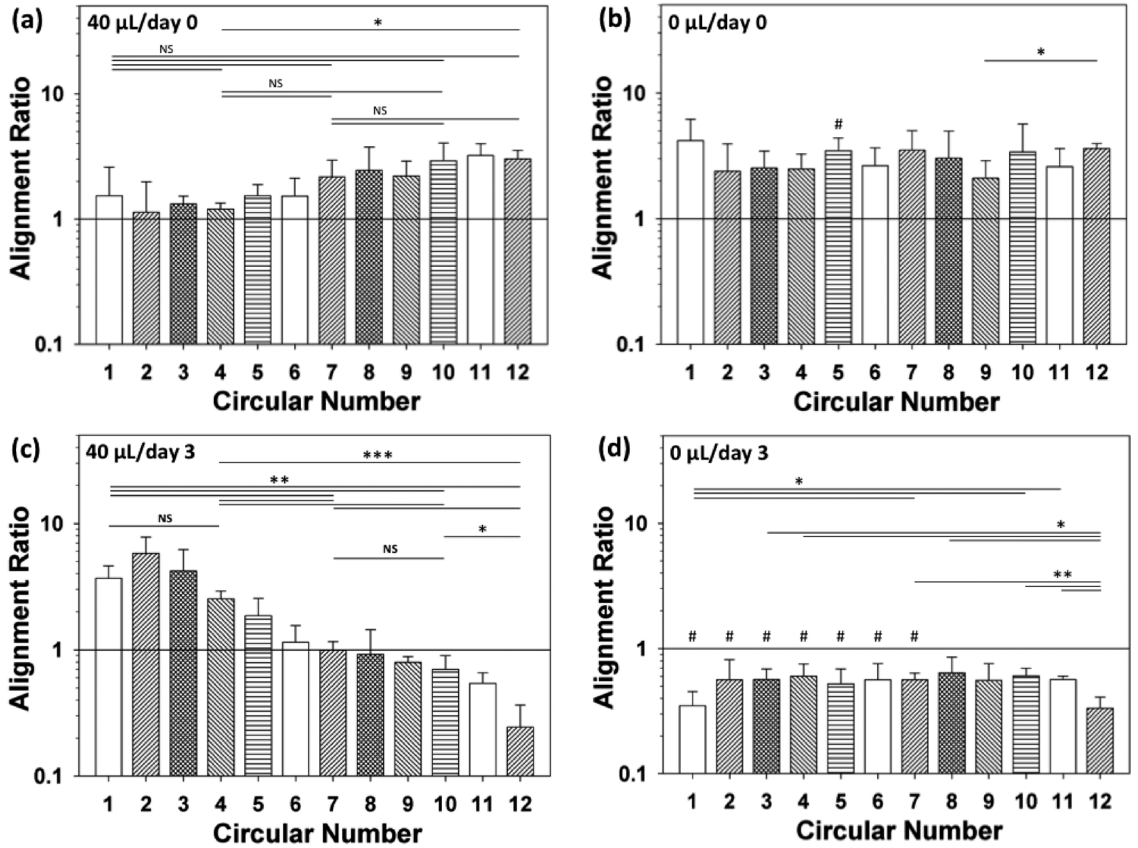


**Fig. 6** $RCA_{ratio}$ of 3T3 cells in the GSS-microChip (a) with the 40 μL injection volume at day 0, (b) with the 0 μL injection volume at day 0, (c) the 40 μL injection volume at day 3, and (d) the 0 μL injection volume at day 3. In (a) and (c), only circles 1, 4, 7, 10, and 12 were analyzed to identify significant differences. (#) indicates a significant difference ($p < 0.05$) between circle number $n$ in the 0 μL injection volume chip and circle number $n$ of the 40 μL injection volume chip on the same day ($n$ = 1–12). (*), (**), and (***) indicate significant differences at $p < 0.05$, 0.01, and 0.001, respectively.

difference ($p < 0.05$) between the 40 μL (Fig. 6(a) and (c)) and 0 μL (Fig. 6(b) and (d)) injection volumes at the same day in Fig. 6(b) and (d).)

The $RCA_{ratio}$ of hydrogels 2–11 for the 0 μL/day 3 condition (Fig. 6(d)) was approximately 0.5, and the values for the hydrogels in the center (hydrogel 1) and at the boundary (hydrogel 12) were approximately 0.3. There were no significant differences among hydrogels 2–11. Only hydrogels 1 and 12 were different from hydrogels 2–11. This difference originates from the smaller line width of hydrogel 1 and 12 (in Fig. 3(d)) due to the diffraction effect (Fig. S-13†);[57,58] therefore, the ratio of the cell size to the hydrogel width was higher for hydrogels number 1 and 12 than for 2–11. The higher ratio of the cell size to the hydrogel width resulted in more long-axis alignment.

## Conclusions

We developed a microfluidic chip with a flexible PDMS membrane to exert gradient strain to produce micropatterned hydrogels. After releasing the applied liquid pressure on the PDMS membrane, the PDMS membrane automatically applies force on the concentric circle-patterned cell-laden hydrogels that results in gradient strain with a maximum at the center and a minimum at the outer boundary. In the GSS-microChip, the 3T3 cells had a radial arrangement with an $RCA_{ratio}$ of ~4.2 in hydrogel 1 (>50% initial compressive strain). The gradual decrease in the initial compressive strain from hydrogel 1 to hydrogel 12 resulted in a gradual decrease in the $RCA_{ratio}$ of the 3T3 cells. In hydrogel number 12, the 3T3 cells had a circular alignment with an $RCA_{ratio}$ of ~0.22 with 5–15% initial compressive strain. The cell viability was higher than 80% from day 0 to day 5. Therefore, the gradient static strain chip can generate an active gradient strain on 3D encapsulated cells in hydrogels to allow for the facile investigation of different cellular behaviors under various conditions of compressive strain/elongation in one chip without the need for external mechanical devices. In addition, this technique can be easily integrated with biochemical or biophysical stimulations for tissue regeneration.

## Acknowledgements

This project was supported by the Graduate Student Study Abroad Program (NSC-101-2917-I-007-010), Biomedical Engineering Program (NSC-101-2221-E-007-032-MY3), and

Nanotechnology National Program (NSC-101-2120-M-007-001), National Science Council of the R.O.C., Taiwan. In addition, the authors thank Dr. Yiling Qiu for the CSP cell isolation and the Xingtian Temple Foundation and CTCI Foundation scholarships for the financial support during H.-Y.H.'s Ph.D. program. A.K. was supported by the Office of Naval Research Young National Investigator Award, the Presidential Early Career Award for Scientists and Engineers (PECASE), the National Science Foundation CAREER Award (DMR 0847287), and the National Institutes of Health (HL099073, EB012597, DE021468, HL092836, DE019024, EB008392, AR057837). A.P. acknowledges postdoctoral award from Fonds Québécois de la Recherche sur la Nature et les Technologies (FRQS, Canada).



## References

1 C. S. Simmons, B. C. Petzold and B. L. Pruitt, *Lab Chip*, 2012, **12**, 3235–3248.
2 H. Aubin, J. W. Nichol, C. B. Hutson, H. Bae, A. L. Sieminski, D. M. Cropek, P. Akhyari and A. Khademhosseini, *Biomaterials*, 2010, **31**, 6941–6951.
3 C. R. Wan, S. Chung and R. D. Kamm, *Ann. Biomed. Eng.*, 2011, **39**, 1840–1847.
4 A. J. Keung, S. Kumar and D. V. Schaffer, *Annu. Rev. Cell Dev. Biol.*, 2010, **26**, 533–556.
5 E. Blaauw, F. A. van Nieuwenhoven, P. Willemsen, T. Delhaas, F. W. Prinzen, L. H. Snoeckx, M. van Bilsen and G. J. van der Vusse, *Am. J. Physiol.*, 2010, **299**, H780–H787.
6 J. T. Butcher, B. C. Barrett and R. M. Nerem, *Biomaterials*, 2006, **27**, 5252–5258, 2006.
7 W. Xiao, J. He, J. W. Nichol, L. Wang, C. B. Hutson, B. Wang, Y. Du, H. Fan and A. Khademhosseini, *Acta Biomater.*, 2011, **7**, 2384–2393.
8 T. C. Lim, W. S. Toh, L. S. Wang, M. Kurisawa and M. Spector, *Biomaterials*, 2012, **33**, 3446–3455.
9 S. D. Joshi and K. Webb, *J. Orthop. Res.*, 2008, **26**, 1105–1113.
10 G. Camci-Unal, J. W. Nichol, H. Bae, H. Tekin, J. Bischoff and A. Khademhosseini, *J. Tissue Eng. Regener. Med.*, 2013, **7**, 337–347.
11 J. A. Burdick and G. D. Prestwich, *Adv. Mater.*, 2011, **23**, H41–H56.
12 B. C. Tai, C. Du, S. Gao, A. C. Wan and J. Y. Ying, *Biomaterials*, 2010, **31**, 48–57.
13 M. H. V. Marion, D. W. J. V. D. Schaft, M.-J. Goumans, F. P. T. Baaijens and C. V. C. Bouten, *Cardiovasc. Res.*, 2012, **93 (suppl 1)**, 79.
14 G. Camci-Unal, D. Cuttica, N. Annabi, D. Demarchi and A. Khademhosseini, *Biomacromolecules*, 2013, **14**, 1085–1092.
15 J. L. Vanderhooft, M. Alcoutlabi, J. J. Magda and G. D. Prestwich, *Macromol. Biosci.*, 2009, **9**, 20–28.
16 Y. Lei, S. Gojgini, J. Lam and T. Segura, *Biomaterials*, 2011, **32**, 39–47.
17 G. Camci-Unal, P. Zorlutuna, and A. Khademhosseini, Fabrication of Microscale Hydrogels for Tissue Engineering Applications, in *Biofabrication*, ed. Forgacs, G. and Sun, W., Elsevier Inc., 2013, pp. 59–80.
18 G. Camci-Unal, H. Aubin, A. F. Ahari, H. Bae, J. W. Nichol and A. Khademhosseini, *Soft Matter*, 2010, **6**, 5120–5126.
19 H. Tian, L. Lin, J. Chen, X. Chen, T. G. Park and A. Maruyama, *J. Controlled Release*, 2011, **155**, 47–53.
20 A. M. Hawkins, T. A. Milbrandt, D. A. Puleo and J. Z. Hilt, *Acta Biomater.*, 2011, **7**, 1956–1964.
21 J. Ramon-Azcon, S. Ahadian, R. Obregon, G. Camci-Unal, S. Ostrovidov, V. Hosseini, H. Kaji, K. Ino, H. Shiku, A. Khademhosseini and T. Matsue, *Lab Chip*, 2012, **12**, 2959–2969.
22 B. C. Kim, H. Bae, I. K. Kwon, E. J. Lee, J. H. Park, A. Khademhosseini and Y. S. Hwang, *Tissue Eng., Part B*, 2012, **18**, 235–244.
23 J. W. Nichol, S. T. Koshy, H. Bae, C. M. Hwang, S. Yamanlar and A. Khademhosseini, *Biomaterials*, 2010, **31**, 5536–5544.
24 F. Piraino, G. Camci-Unal, M. J. Hancock, M. Rasponi and A. Khademhosseini, *Lab Chip*, 2012, **12**, 659–661.
25 V. Hosseini, S. Ahadian, S. Ostrovidov, G. Camci-Unal, S. Chen, H. Kaji, M. Ramalingam and A. Khademhosseini, *Tissue Eng., Part A*, 2012, **18**, 2453–2465.
26 C. Nakanishi, M. Yamagishi, K. Yamahara, I. Hagino, H. Mori, Y. Sawa, T. Yagihara, S. Kitamura and N. Nagaya, *Biochem. Biophys. Res. Commun.*, 2008, **374**, 11–16.
27 D. Dado, M. Sagi, S. Levenberg and A. Zemel, *Regener. Med.*, 2012, **7**, 101–116.
28 E. Serena, E. Cimetta, S. Zatti, T. Zaglia, M. Zagallo, G. Keller and N. Elvassore, *PLoS One*, 2012, **7**, e48483.
29 Y. K. Luu, E. Capilla, C. J. Rosen, V. Gilsanz, J. E. Pessin, S. Judex and C. T. Rubin, *J. Bone Miner. Res.*, 2009, **24**, 50–61.
30 D. Huh, B. D. Matthews, A. Mammoto, M. Montoya-Zavala, H. Y. Hsin and D. E. Ingber, *Science*, 2010, **328**, 1662–1668.
31 X. Li, J. S. Chu, L. Yang and S. Li, *Ann. Biomed. Eng.*, 2012, **40**, 598–605.
32 K. Unno, M. Jain and R. Liao, *Circ. Res.*, 2012, **110**, 1355–1363.
33 V. F. Segers and R. T. Lee, *Nature*, 2008, **451**, 937–942.
34 J. Guan, F. Wang, Z. Li, J. Chen, X. Guo, J. Liao and N. I. Moldovan, *Biomaterials*, 2011, **32**, 5568–5580.
35 Z. Ma, Q. Liu, H. Liu, H. Yang, J. X. Yun, C. Eisenberg, T. K. Borg, M. Xu and B. Z. Gao, *Lab Chip*, 2012, **12**, 566–573.
36 C. Y. Chung, H. Bien and E. Entcheva, *J. Cardiovasc. Electrophysiol.*, 2007, **18**, 1323–1329.
37 F. Patolsky, B. P. Timko, G. Yu, Y. Fang, A. B. Greytak, G. Zheng and C. M. Lieber, *Science*, 2006, **313**, 1100–1104.
38 R. A. Gould, K. Chin, T. P. Santisakultarm, A. Dropkin, J. M. Richards, C. B. Schaffer and J. T. Butcher, *Acta Biomater.*, 2012, **8**, 1710–1719.
39 J. Foolen, V. S. Deshpande, F. M. Kanters and F. P. Baaijens, *Biomaterials*, 2012, **33**, 7508–7518.
40 J. I. Luna, J. Ciriza, M. E. Garcia-Ojeda, M. Kong, A. Herren, D. K. Lieu, R. A. Li, C. C. Fowlkes, M. Khine and K. E. McCloskey, *Tissue Eng., Part C*, 2011, **17**, 579–588.

 

41 A. R. Nectow, E. S. Gil, D. L. Kaplan and M. E. Kilmer, A statistical algorithm for assessing cellular alignment *J. Biomed. Mater. Res., Part A*, 2013, **101**, 884–891.
42 B. V. Slaughter, S. S. Khurshid, O. Z. Fisher, A. Khademhosseini and N. A. Peppas, *Adv. Mater.*, 2009, **21**, 3307–3329.
43 N. O. Chahine, G. A. Ateshian and C. T. Hung, *Biomech. Model. Mechanobiol.*, 2007, **6**, 103–111.
44 S. H. Park, W. Y. Sim, B. H. Min, S. S. Yang, A. Khademhosseini and D. L. Kaplan, *PLoS One*, 2012, **7**, e46689.
45 K. Kurpinski, J. Chu, C. Hashi and S. Li, *Proc. Natl. Acad. Sci. U. S. A.*, 2006, **103**, 16095–16100.
46 W. Y. Sim, S. W. Park, S. H. Park, B. H. Min, S. R. Park and S. S. Yang, *Lab Chip*, 2007, **7**, 1775–1782.
47 D. Vader, A. Kabla, D. Weitz and L. Mahadevan, *PLoS One*, 2009, **4**, e5902.
48 Y. S. Hwang, B. G. Chung, D. Ortmann, N. Hattori, H. C. Moeller and A. Khademhosseini, *Proc. Natl. Acad. Sci. U. S. A.*, 2009, **106**, 16978–16983.
49 B. A. Aguado, W. Mulyasasmita, J. Su, K. J. Lampe and S. C. Heilshorn, *Tissue Eng., Part A*, 2012, **18**, 806–815.
50 J. Wan, *Polymers*, 2012, **4**, 1084–1108.
51 C. Moraes, G. Wang, Y. Sun and C. A. Simmons, *Biomaterials*, 2010, **31**, 577–584.
52 O. Pfister, F. Mouquet, M. Jain, R. Summer, M. Helmes, A. Fine, W. S. Colucci and R. Liao, *Circ. Res.*, 2005, **97**, 52–61.
53 H.-Y. Hsieh, P.-C. Wang, C.-L. Wu, C.-W. Huang, C.-C. Chieng and F.-G. Tseng, *Anal. Chem.*, 2009, **81**, 7908–7916.
54 H.-Y. Hsieh, T.-W. Huang, J.-L. Xiao, C.-S. Yang, C.-C. Chang, C.-C. Chu, L.-W. Lo, S.-H. Wang, P.-C. Wang, C.-C. Chieng, C.-H. Lee and F.-G. Tseng, *J. Mater. Chem.*, 2012, **22**, 20918–20928.
55 A. I. Teixeira, G. A. Abrams, P. J. Bertics, C. J. Murphy and P. F. Nealey, *J. Cell Sci.*, 2003, **116**, 1881–1892.
56 T. Nakajima, T. Kurokawa, S. Ahmed, W.-l. Wu and J. P. Gong, *Soft Matter*, 2013, **9**, 1955–1966.
57 Y.-J. Chuang, F.-G. Tseng, J.-H. Cheng and W.-K. Lin, *Sens. Actuators, A*, 2003, **103**, 64–69.
58 R. Yang and W. Wang, *Sens. Actuators, B*, 2005, **110**, 279–288.
59 J. Eyckmans, G. L. Lin and C. S. Chen, *Biol. Open*, 2012, **1**, 1058–1068.
60 V. Chan, M. B. Collens, J. H. Jeong, K. Park, H. Kong and R. Bashir, *Virtual Phys. Prototyp.*, 2012, **7**, 219–228.